AGU100 ADVANCING EARTH AND SPACE SCIENCE

Journal of Advances in Modeling Earth Systems

RESEARCH ARTICLE
10.1002/2017MS001226

Key Points:
- We propose a novel, hybrid approach for cloud microwave scattering properties in CRTM
- We use nonspherical particles to replace some selected microphysics-specified soft spheres
- The hybrid approach reduces the inconsistency of interchannel CRTM radiances using only spherical particle properties

Correspondence to:
F. Zhang,
fzhang@psu.edu

Citation:
Sieron, S. B., Zhang, F., Clothiaux, E. E., Zhang, L. N., & Lu, Y. (2018). Representing precipitation ice species with both spherical and nonspherical particles for radiative transfer modeling of microphysics-consistent cloud microwave scattering properties. *Journal of Advances in Modeling Earth Systems*, *10*, 1011–1028. https://doi.org/10.1002/2017MS001226

Received 1 NOV 2017
Accepted 22 MAR 2018
Accepted article online 30 MAR 2018
Published online 13 APR 2018

Representing Precipitation Ice Species With Both Spherical and Nonspherical Particles for Radiative Transfer Modeling of Microphysics-Consistent Cloud Microwave Scattering Properties

Scott B. Sieron[1], Fuqing Zhang[1], Eugene E. Clothiaux[1], Lily N. Zhang[1,2], and Yinghui Lu[1]

[1]Department of Meteorology and Atmospheric Science, and Center for Advanced Data Assimilation and Predictability Techniques, Pennsylvania State University, University Park, PA, USA, [2]State College Area High School, State College, PA, USA

Abstract Cloud microwave scattering properties for the Community Radiative Transfer Model (CRTM) have previously been created to be consistent with the particle size distributions specified by the WSM6 single-moment microphysics scheme. Here substitution of soft sphere scattering properties with nonspherical particle scattering properties is explored in studies of Hurricane Karl (2010). A nonsphere replaces a sphere of the same maximum dimension, and the number of particles of a given size is scaled by the ratio of the sphere to nonsphere mass to keep the total mass of a given particle size unchanged. The replacement of homogeneous soft sphere snow particles is necessary to resolve a highly evident issue in CRTM simulations: precipitation-affected brightness temperatures are generally warmer at 183 GHz than at 91.7 GHz, whereas the reverse is seen in observations. Using sector snowflakes resolve this issue better than using columns/plates, bullet rosettes, or dendrites. With sector snowflakes, both of these high frequencies have low simulated brightness temperatures compared to observations, providing a clear and consistent suggestion that snow is being overproduced in the examined simulation using WSM6 microphysics. Graupel causes cold biases at lower frequencies which can be reduced by either reducing graupel water contents or replacing the microphysics-consistent spherical graupel particles with sector snowflakes. However, soft spheres are likely the better physical representation of graupel particles. The hypotheses that snow and graupel are overproduced in simulations using WSM6 microphysics shall be examined more systematically in future studies through additional cases and ensemble data assimilation of all-sky microwave radiance observations.

1. Introduction

Observations from passive microwave radiometers in low-Earth orbit provide valuable information regarding tropical cyclone structure below cloud top. Brightness temperature measurements contain information on temperature perturbations in the cyclone warm core (e.g., Brueske & Velden, 2003), relate to surface wind (e.g., Meissner & Wentz, 2009), and inform on the amount and location of liquid and ice water contents of clouds and precipitation (e.g., Alvey et al., 2015; Harnos & Nesbitt, 2016; Reul et al., 2017; Rozoff et al., 2015). The latter directly relate to latent heat release, the fundamental energy source for tropical cyclones. Compared to other instruments deployed, satellite microwave radiometers take more measurements across all tropical oceans that directly relate to tropical cyclone latent heat release. Thus, effective assimilation of precipitation-affected passive microwave observations in the analyses of regional-scale tropical cyclone numerical models may lead to improvements in forecasts (e.g., Haddad et al., 2015; Madhulatha et al., 2017; Yang et al., 2016).

Significant challenges in assimilating precipitation-affected brightness temperatures have involved the use of a radiative transfer model as the observation operator, particularly the effects of ice scattering (e.g., Kulie et al., 2010). In Sieron et al. (2017), microwave scattering lookup tables for clouds and precipitation for the Community Radiative Transfer Model (CRTM; Han et al., 2006) were constructed to ensure that simulations are consistent with the respective particle properties (i.e., homogenous spheres) and size distributions specified by the WRF 6-Species Single-Moment (WSM6; Dudhia et al., 2008), Goddard (Lang et al., 2007), and

Morrison (Morrison et al., 2009) microphysics schemes in the Weather Research and Forecasting (WRF) model (Skamarock et al., 2008). For the particle sizes, D, of the precipitation species (rain, snow, and graupel, which are responsible for most of the departures from clear-sky brightness temperatures), all three schemes use a gamma distribution,

$$N(D)\left[\mathrm{m}^{-3}\ \mathrm{m}^{-1}\right]=N_0 D^{\mu} e^{-\lambda D}, \tag{1a}$$

with

$$\lambda=\left(\frac{\pi\rho N_0\Gamma(\mu+1)}{\rho_a q}\right)^{1/4}, \tag{1b}$$

and

$$N_0=\frac{N\lambda^{\mu+1}}{\Gamma(\mu+1)}, \tag{1c}$$

with the shape parameter $\mu=0$, otherwise known as an exponential distribution. Implicit to this specific form of gamma distribution in models is the assumption that particle mass is proportional to the cube of its size, or that particles are spheres with a bulk density, ρ, that is independent of particle size/mass. In WSM6, graupel has a bulk density of 500 kg m^{-3}, and snow 100 kg m^{-3}. Thus, "distribution-specific" cloud scattering properties for a given water content were calculated by Sieron et al. (2017) through integrating the product of the microphysics particle size distribution and the scattering properties of homogeneous spheres of the specified bulk density. Such "distribution-specific" lookup tables (CRTM-DS) improve upon consistency with a microphysics scheme compared to the default approach of the CRTM (CRTM-RE) because clouds with different particle size distributions but equal values of effective radii (ratio of the third and second moments of the particle size distribution) can have different microwave scattering properties, and the bulk density of an ice species in the microphysics scheme may not have corresponding entries in the lookup table (such as with WSM6 graupel; see Sieron et al., 2017).

Differences in cloud scattering properties between the new CRTM-DS and existing CRTM-RE lookup tables—perhaps due to inconsistencies in the particle size distribution between the microphysics and the CRTM-RE lookup table—result in much lower simulated brightness temperatures from the former (Sieron et al., 2017). But both approaches produced inconsistent brightness temperatures across several frequencies as compared with observations. Specifically, the generally colder CRTM-DS simulations resulted in a cold bias at frequencies 91.7 GHz and below, while the generally warmer CRTM-RE produced a far more substantial warm bias at 183 $\pm$ 7 GHz. Other studies using microphysics-consistent hydrometeor scattering applied to WRF output (Han et al., 2013; Masunaga et al., 2010) and other cloud-resolving models (e.g., Li et al., 2010; Matsui et al., 2016) have found cold biases at 91.7 GHz or other frequencies in the W band.

Both the CRTM-DS and CRTM-RE approaches are implemented using spherical particles to represent the scattering properties of ice species. While this is appropriate for a simulator of a microphysical scheme that assumes spherical particles, it is possible—if not likely—that the inconsistencies by frequency relative to observations seen in the CRTM-DS and CRTM-RE results are inherent to the use of spherical particle scattering properties. Several studies have documented the shortcomings in using ice spheres in estimating the optical properties of real ice particles, many of which are not spherical in shape (e.g., Baran et al., 2011; Geer & Baordo, 2014; Hong, 2007; Liu, 2008). Eriksson et al. (2015) provide a comprehensive investigation of the likely challenges with applying spherical and spheroidal particle scattering, even if bulk density is not prescribed to a constant microphysics-specified value but is tuned by frequency (e.g., Liu, 2004) or with different size particles (e.g., Hogan et al., 2012) in an effort to produce simulations in better agreement with observations. For example, the simulations in Surussavadee and Staelin (2007), which use spherical snow and graupel particles with tuned wavelength-dependent bulk densities, have a cold bias to observations at 89 GHz and a slight warm bias at 183 $\pm$ 7 GHz among scenes classified convective or tropical.

In Geer and Baordo (2014), the RTTOV-SCATT radiative transfer model was modified to use nonspherical ice particles for snow (the only precipitation ice species in the model) instead of soft spheres, and several habits were found to produce a better correspondence between observations and simulations from ECMWF 4D-Var global analyses; their development of precipitation-affected radiance assimilation has continued (e.g.,

Kazumori et al., 2016). More recently, Galligani et al. (2017) applied the scattering properties of nonspherical particles to soft spheres in the particle size distributions of a selection of WRF microphysics schemes to compare simulations of South American thunderstorms.

In this work, nonspherical ice particle scattering properties are used to replace those from ice spheres in microphysics-consistent cloud scattering property calculations in Community Radiative Transfer Model (CRTM) microwave simulations of high-resolution tropical cyclone forecasts. Using nonspherical particle representations of snow and graupel effectively relaxes, but does not wholly abandon, the simulator ideals of strict consistency between the radiative transfer and the model microphysics scheme particle properties including size distributions. Moreover, doing so will be shown to produce brightness temperatures which are more consistent with observations across a greater range of microwave frequencies, especially when allowing for adjustments—perhaps bias correction—of precipitation ice water contents that are possible with data assimilation.

2. Setup of Models

The WRF model was run to produce high-resolution forecasts of Hurricane Karl (2010) during rapid intensification in the Bay of Campeche from 22 UTC 16 September to 15 UTC 17 September. Following Sieron et al. (2017), the WRF simulations were initialized with an ensemble Kalman filter analysis assimilating airborne Doppler radar radial velocity observations as presented in Melhauser et al. (2017) with the methodologies developed in Zhang and Weng (2015) and Weng and Zhang (2012). The WSM6 (Dudhia et al., 2008) microphysics scheme was used; the scheme has liquid cloud, rain, ice cloud, snow, and graupel hydrometeor species. Further description of the initial conditions and WRF configurations are provided in Sieron et al. (2017).

The hourly output of the 3 km grid spacing domain served as input to the Community Radiative Transfer Model (CRTM) with the Successive Order of Interactions solver (Greenwald et al., 2004) and 16 + 2 streams enabled for all profiles. First, brightness temperatures were simulated with cloud scattering properties calculated using the particle properties (i.e., homogenous spheres) and size distributions specified by the microphysics scheme (via CRTM-DS; Sieron et al., 2017). Then brightness temperatures were simulated after replacing the soft sphere scattering properties for either one or two of the precipitation ice species with those from nonspherical particles (as described in the following paragraphs). The 3 km grid spaced simulated brightness temperatures were convolved to the locations observed by the Defense Meteorological Satellite Program (DMSP) F-16 SSMIS overpass at 0113 UTC 17 September using a simple symmetric Gaussian weighting function (Bennartz, 2000; see Sieron et al., 2017). The average effective field of view for SSMIS on a DMSP satellite varies from about 57.7 km at 19.35 GHz to 14.4 km at 183.31 GHz.

3. Nonspherical Particles

The database of nonspherical particle scattering properties developed by Liu (2008) was utilized. This database includes absorption and scattering properties of five columns and plates, four rosettes, and two snowflake models. Consistent with CRTM-DS lookup table construction, the scattering and absorption properties of the database used here are valid at a temperature of 273.15 K; the CRTM otherwise models cloud absorption and emission assuming cloud temperature is equal to the surrounding air temperature.

The associated database of aggregate particles (Nowell et al., 2013) was not considered because scattering phase functions are not provided with this database at this time. Due to strong evidence of multiple scattering in the CRTM simulations, the choice was made to use exact phase functions of particles in calculating cloud scattering phase functions for these 16 + 2 stream simulations instead of applying a parameterization (e.g., Liu & Weng, 2006).

This study explores the use of nonspherical particle shapes to represent the scattering properties of snow and graupel, but not for the ice cloud species. Small nonprecipitating ice cloud particles are represented as spheres in the CRTM-DS, and they have minimal impact on brightness temperatures up to 183 GHz. Experiments on the sensitivity of brightness temperatures on individual ice species were run with the CRTM-DS for the WRF simulation of Hurricane Karl at 0100 UTC 17 September. If snow and graupel are entirely removed from the CRTM input, then the additional removal of all ice clouds produces an increase in 183 ± 7 GHz convolved brightness temperatures of 0.65 K averaged across all locations with more than the

median ice cloud water path (0.0232 kg m^{-2}), and no more than 2.7 K at any single location. See section 5 for further discussion on WSM6 ice clouds.

As mentioned in section 1, the WSM6 microphysics scheme, like many bulk microphysics schemes, specifies that the mass of a snow or graupel particle is proportional to its volume according to a bulk density, ρ. The power law relationship between particle maximum dimension, D, and particle mass, m, is

$$m(D) = aD^b, \tag{2}$$

with $b=3$ and $a=\frac{\pi}{6}\rho$ for spheres. All of the various bullet rosette and snowflake particle constructions in the Liu (2008) database represent the growths of ice particle types in a more natural way: particle mass generally relates to maximum dimension by a power, b, less than three (e.g., Mitchell, 1991; Szyrmer & Zawadzki, 2010), specifically between about 2.37 and 1.58 for these Liu particles (Kulie et al., 2010).

Because of this mass-size relationship inconsistency, a method must be devised for replacing the WSM6 microphysics soft spheres with the nonspherical particles in the Liu database for calculating new cloud scattering properties. This subject has been similarly discussed by Galligani et al. (2017), Geer and Baordo (2014), and Eriksson et al. (2015). Here we discuss two classes of methods, one based on replacing particles of equal mass, and the other based on replacing particles of equal maximum dimension (which has three variants).

3.1. Replacement by Particle Mass and Integration Truncation

The microwave scattering of a snow and graupel particle may be best described as primarily a function of its mass, m, or the total number of water molecule dipoles; across the particle size distribution of precipitation, there is generally greater similarity in microwave scattering and absorption between particles of the same mass than particles of the same maximum dimension (e.g., Eriksson et al., 2015). It follows that the most natural approach to allow for the expression of differences in scattering between particles of different shapes is to substitute between particles of the same mass, as done by Galligani et al. (2017). This method sidesteps some of the complications from differences in the mass-diameter relationship by not addressing consistency with the particle size distribution. Instead, the new collection of particles would be consistent with the original microphysics specification of the particle mass distribution, $N(m)$, and, by extension, the total mass of all particles of a given mass, $M(m)=mN(m)$, and the total water content.

An issue with this approach arises with the WSM6 scheme at moderate and high values of water contents, as a substantial percentage of the modeled snow or graupel is contained in particles of mass that exceed the upper bound of many particle shapes in the Liu database. For example, 1 g m^{-3} of WSM6 snow with intercept parameter 1.56×10^7 m^{-3} m^{-1} (valid for 256 K) would have 39.9% of the total mass contained in particles of mass greater than 1.16 mg (soft sphere diameter of 2.81 mm), which is the maximum mass of the Liu (2008) sector snowflake particle type (maximum dimension of 10 mm). This raises the problem as to how to assign scattering properties to modeled particles with a mass exceeding the upper limit of the database. If calculating mass-weighted extinction coefficients and single-scattering albedos (e.g., for CRTM lookup tables), one simple solution to this issue would be to use the numerically truncated estimate of the water content instead of the original water content. This substitution is equivalent in purpose and effect to the rescaling of the particle size distribution described in Geer and Baordo (2014, Appendix C).

However, these mass renormalization procedures do not resolve all consequences of integration truncation. These procedures replace the truncated collection of large and massive particles with a greater collection of smaller particles, and this new collection of particles will interact with radiation differently. Illustrating this effect with a spherical particle scattering database (see Sieron et al., 2017), Figure 1 shows that substantially different values of scattering coefficients and asymmetry parameters for moderate and high water contents of WSM6 snow and graupel are produced when truncating the integration at the maximum mass of the Liu sector snowflake. While these results are based on soft spheres, similar results are expected for nonspherical particles. For microphysics schemes which produce an inaccurate total mass of massive particles, this truncation can be an unintentional bias correction in the forward model.

3.2. Replacement by Particle Maximum Dimension

This largely unresolvable issue of integration truncation with WSM6 particle size distributions and the Liu particle scattering database, especially with the bullet rosette and snowflake particle types, must be better

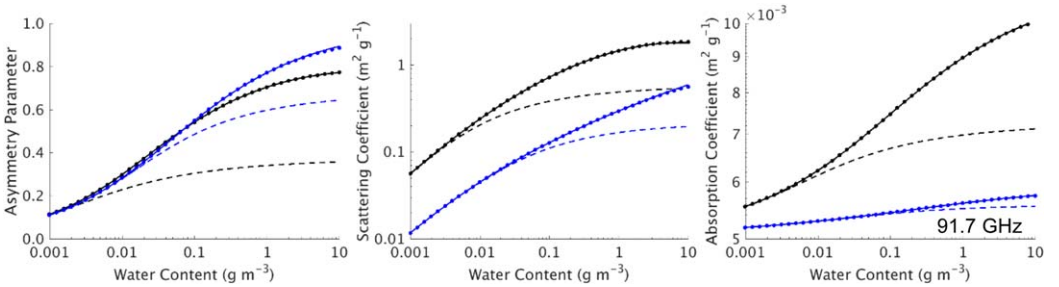

Figure 1. Illustration of the impact of integration truncation on mass-weighted scattering and absorption properties at 91.7 GHz for graupel (black) and snow (blue) species according to the specifications of the WSM6 microphysics scheme with spheres of bulk density 500 kg m^{-3} for graupel and 100 kg m^{-3} for snow. Solid lines show integration up to a soft sphere diameter of 20 mm, which is the largest sphere in the spherical particle scattering database. Dotted lines, which fall atop of the solid lines, show integration up to a soft sphere diameter of 10 mm, corresponding to the largest Liu (2008) sector snowflake and bullet rosette. Dashed lines show integration up to a soft sphere mass of 1.16 mg, corresponding to the most massive sector snowflake. Scattering and absorption coefficients are for ice particles with a temperature of 273.15 K. An intercept parameter of 1.56×10^7 m^{-3} m^{-1} is assumed for the WSM6 snow particle size distribution.

managed. A second approach is to substitute particles with respect to maximum dimension. The range of maximum dimensions in the Liu database allows for cloud scattering calculations at high water contents which are representative of the microphysics specifications; a similar confidence is expressed by Geer and Baordo (2014). For example, all four of the bullet rosettes and both snowflake types extend to maximum dimensions of at least 10 mm. Figure 1 shows that integration truncation out to this particle diameter has a negligible impact, as there is virtually no difference in results when comparing to those from integration out 20 mm diameters. What follows are descriptions of three different methods of particle replacement by maximum dimension.

In Geer and Baordo (2014), the particle size distribution of the replacing nonspherical particles is imposed to match the original total water content (hydrometeor mass per unit volume), I, of the snow species. The total mass of particles of a given size,

$$M(D)=m(D)N(D), \tag{3}$$

is integrated over all particle sizes to calculate the total water content. If $m(D)$ for a given particle type follows a power law (equation (2))—or, if not, a best fit estimate of the parameters a and b is produced—then this integration is

$$I=\int_0^\infty aD^bN(D)dD. \tag{4}$$

As the two particle types will have different values of a and b, the imposed equality in total water content is achieved by changing the value or formulation of the free parameter of the particle size distribution. Snow in RTTOV-SCAT (Geer & Baordo, 2014) has an exponential particle size distribution (equation (1a) with shape parameter $\mu=0$) with the slope, λ, as the free parameter, which relates to a, b, the intercept parameter N_0, and the water content by

$$\lambda=\left(\frac{\Gamma(b+1)aN_0}{I}\right)^{(b+1)^{-1}}. \tag{5}$$

A different substitution method would be to impose that the new distribution of nonspherical particles matches the original particle size distribution, $N(D)$: *one* new particle replaces *one* original particle of the same maximum dimension. In this sense, this method chooses to completely ignore any difference in mass-dimension relationship between the two particle types. This would lead to inconsistencies between the new and original total water contents. However, this can be corrected by rescaling the particle size distribution by the ratio of the new and original total water content (the equivalent rescaling procedure for integration truncation). This rescaling of the particle size distribution to revert back to the original water content effectively treats the parameter relating to the number concentration as free, which for a gamma distribution is the intercept parameter.

Yet another possible substitution method would be to impose consistency with the total mass of a particle population with respect to size, $M(D)$. This differs from the method in Geer and Baordo (2014) in which consistency is imposed only with the integral of this function, i.e., the total water content. To preserve $M(D)$, original particles of a given size would be replaced by new particles of that size, but the number of particles of that size would be scaled by the ratio of the mass of the original particle to the mass of the new particle that replaces it. For example, if the microphysics scheme specifies there to be 20 ice spheres in the bin corresponding to a particle diameter of 1 mm, and this sphere has 3 times the mass of the nonspherical particle with maximum dimension 1 mm, then the 20 spheres would be replaced with 60 of the nonspheres. Using a prime to denote that which is valid for the new particle type, then setting $M'(D)=M(D)$ gives

$$N'(D)=\frac{m(D)}{m'(D)}N(D). \tag{6}$$

If $m(D)$ for both particle types follows a power law, and the particle size distribution is gamma, then the new gamma distribution for the new particle types is

$$N'(D)=\frac{a}{a'}N_0D^{(\mu+b-b')}e^{-\lambda D}. \tag{7}$$

In this method, intercept and shape parameters of the particle size distribution are free, while the slope parameter is fixed.

This scaling by relative particle mass is entirely appropriate if the scattering cross section of a particle of a given size is primarily related linearly to its mass, and secondarily to its shape. Granted, this is generally not the case. For example, the scattering cross sections of particles much smaller than the wavelength are in fact proportional to the square of the mass. In an extreme example, substituting 200 particles of size 0.2 mm and mass 10^{-4} mg (total scattering proportional to 200×10^{-24}) with 20 particles of size 0.2 mm and mass 10^{-3} mg (total scattering proportional to 20×10^{-18}) preserves the total mass of particles this size. But instead of keeping the total scattering approximately the same (except for the impacts of a different particle shape), this substitution increases the scattering by a factor of 10^5. However, smaller snow and graupel particles have such small scattering cross sections that the overall impact of these substitutions on the brightness temperatures at most frequencies is likely to be low compared to the impact of all of the larger particles. The maxima of the total mass of particles of a given size, $M(D)$, for significant snow and graupel water contents correspond well with the maxima in the mass-weighted scattering coefficients at the frequencies measured by SSMIS (e.g., Sieron et al., 2017, Figure 1), and these particle sizes are not much smaller than, but comparable to, the wavelength. For particle habits with a mass-dimension relationship exponent of 2 for maximum dimensions much greater than the wavelength, then the scattering cross sections of these particles are, indeed, foremost linearly related to their mass and secondarily to their shape.

The pros and cons of different particle replacement methods likely deserve greater consideration and investigation beyond the scope of this work. There appear to be compromises between maximizing the consistency of scattering by particles of the same size/mass but different shape, the distribution of particle sizes/masses as it relates to the relationship between particle size/mass and scattering, the free parameter of the particle size distribution, and perhaps other considerations.

In this work, the driving factors were minimizing integration truncation, and maintaining as much consistency as possible with the physically relevant WSM6 microphysics scheme specifications. Perhaps most significant is consistency with the original cloud mass-weighted average fall speed, which requires preserving the original distribution of total mass with respect to size, $M(D)$. The method employed in this study, which maintains consistency with $M(D)$, is replacement by particles with equal maximum dimension and scaling the number of particles by the relative mass. Further discussion of the relationship between particle shapes and fall speeds, both real and modeled, is provided in section 5.

Figure 2 demonstrates that cloud scattering and absorption properties for WSM6 snow and graupel vary significantly with not only water content, but also between the use of the original spheres and various habits of nonspherical particles in the Liu database. For all properties and at most water contents, ice spheres produce property values that are extrema. This figure is further discussed in the following section in the context of the simulated brightness temperatures.

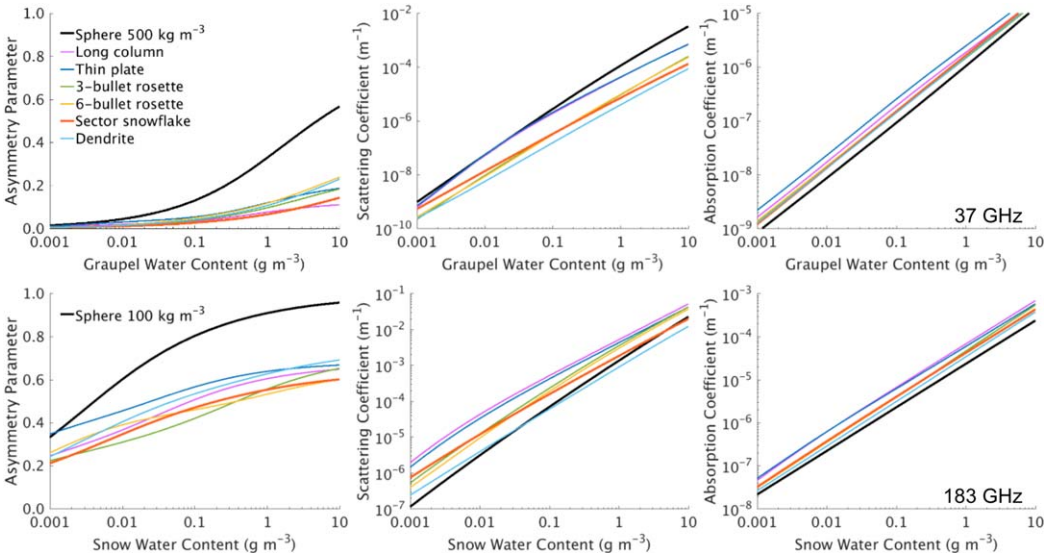

Figure 2. Scattering and absorption property values as a function of ice water content for (top row) graupel (37 GHz) and (bottom row) snow (183 GHz) according to the specifications of the WSM6 microphysics scheme. The use of spheres with bulk density specified by WSM6 is compared to the use of a selection of Liu (2008) database nonspherical particles, with all ice at 273.15 K. The particle size distributions used in each of the nonspherical particle calculations ensures consistency with WSM6-specified total mass with respect to size, $M(D)$. An intercept parameter of 1.56×10^7 m^{-3} m^{-1} (consistent with a temperature of 256 K) is assumed for the WSM6 snow particle size distribution.

4. Results

Figures 3–6 illustrate brightness temperatures (based on horizontally polarized radiances) at the four frequencies of 183 ± 7, 37, 19.35, and 91.7 GHz, respectively, observed by the F16 SSMIS (plot a) and simulated by the CRTM at 0100 UTC 17 September in five different experiments. First, the CRTM-DS lookup tables (with spheres of bulk density specified by the microphysics scheme) for all three ice species are used (plot b). These results are compared to simulations in which spheres are substituted with sector snowflakes by replacement of particles of equal maximum dimension and scaling the number of particles by their relative mass (see equation (7)); this substitution is first applied to both ice precipitation species (snow and graupel; plot c), then only to the snow species (plot d). The appropriateness of this nonspherical particle substitution for graupel is discussed further in section 5. With this in mind, the two additional experiments shown in these figures use sector snowflake scattering properties for only the snow species and demonstrate the impact of halving the water contents of either snow or graupel (plots e and f).

Table 1 provides a summary of all of the CRTM experiments, including domain-averaged brightness temperatures at the four frequencies. Note that the magnitudes of average brightness temperature differences across the whole domain are less than the average brightness temperature differences exclusively over areas of precipitation (not shown). The observations and results of some of these experiments are summarized with histograms (uniform bin width of 5 K) in Figure 7. Figure 8 shows liquid, snow and graupel water paths convolved to the SSMIS 91.7 GHz observation locations using the corresponding effective field of view. These water paths illustrate the spatial distributions of the important hydrometeor types and are of value later on in interpreting simulated brightness temperatures.

4.1. Sector Snowflakes

At SSMIS channel 9 (183 ± 7 GHz; Figures 3 and 7d), CRTM-DS gives a slight warm bias to observed brightness temperatures in the hurricane precipitation area (center of the domain; Figure 3b versus Figure 3a, less area of deep blue). Substituting the snow species spheres with sector snowflakes substantially lowers the brightness temperatures (Figure 3d versus Figure 3b, more areas of deep blue) by a domain-average of 6.8 K. As seen in Figure 2 (bottom row), using sector snowflake scattering properties for the snow species leads to more scattering compared to spheres for nearly all realistic snow water contents, and this scattering is significantly less in the forward direction (smaller asymmetry parameters). Both factors suggest that

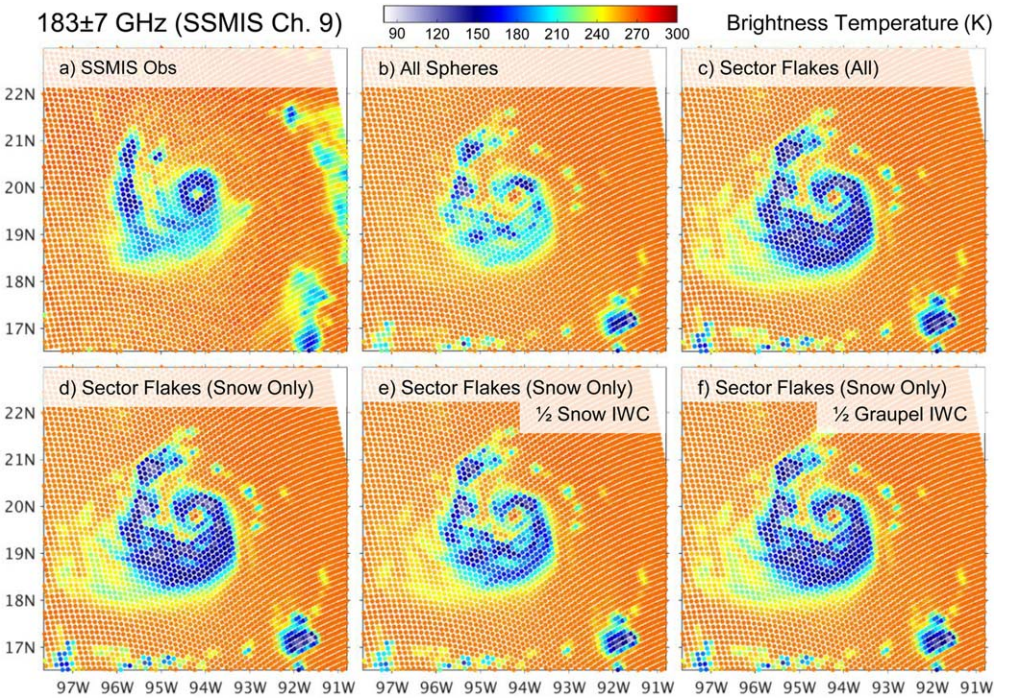

Figure 3. CRTM-simulated (17 September 0100 UTC) and (a) F16 SSMIS observed brightness temperatures (K) at SSMIS channel 9 (183 ± 7 GHz). (b) Uses cloud scattering properties with microphysics-consistent spheres for all ice species (CRTM-DS). (c, d) Results when spheres are substituted with sector snowflakes for all ice precipitation species (snow and graupel) and for only the snow species, respectively. (e, f) Use the same cloud scattering properties as Figure 3d (only the snow species using sector snowflake scattering properties) but with half of the snow and graupel water content, respectively.

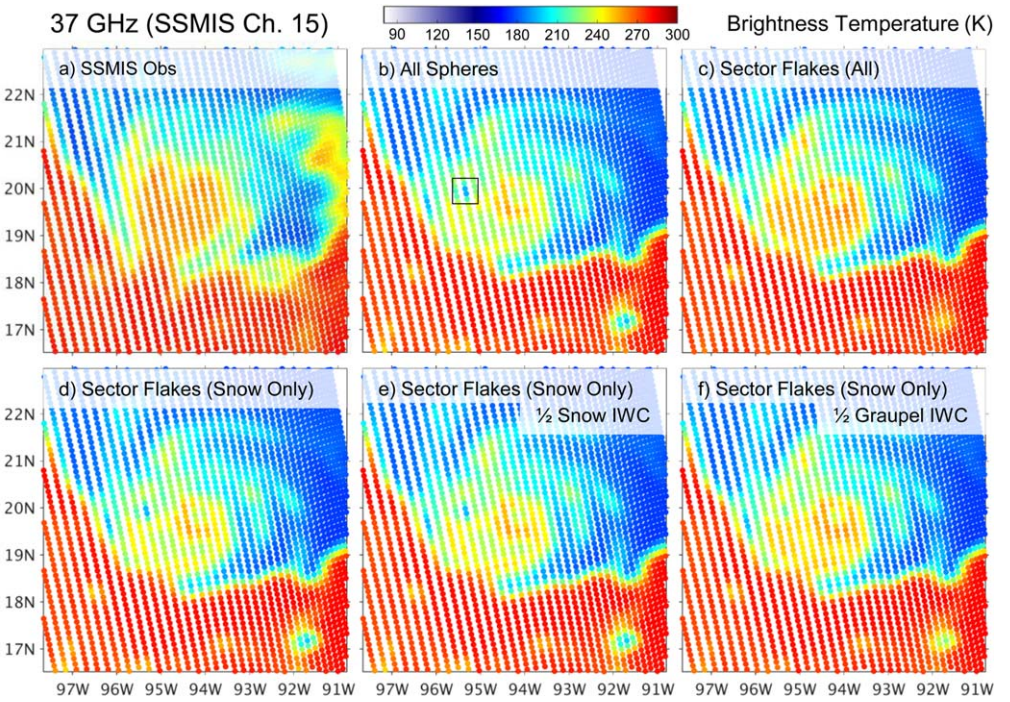

Figure 4. Same as Figure 3 but for SSMIS channel 15 (37 GHz). The box in (b) indicates a location of exceptionally high graupel water path.

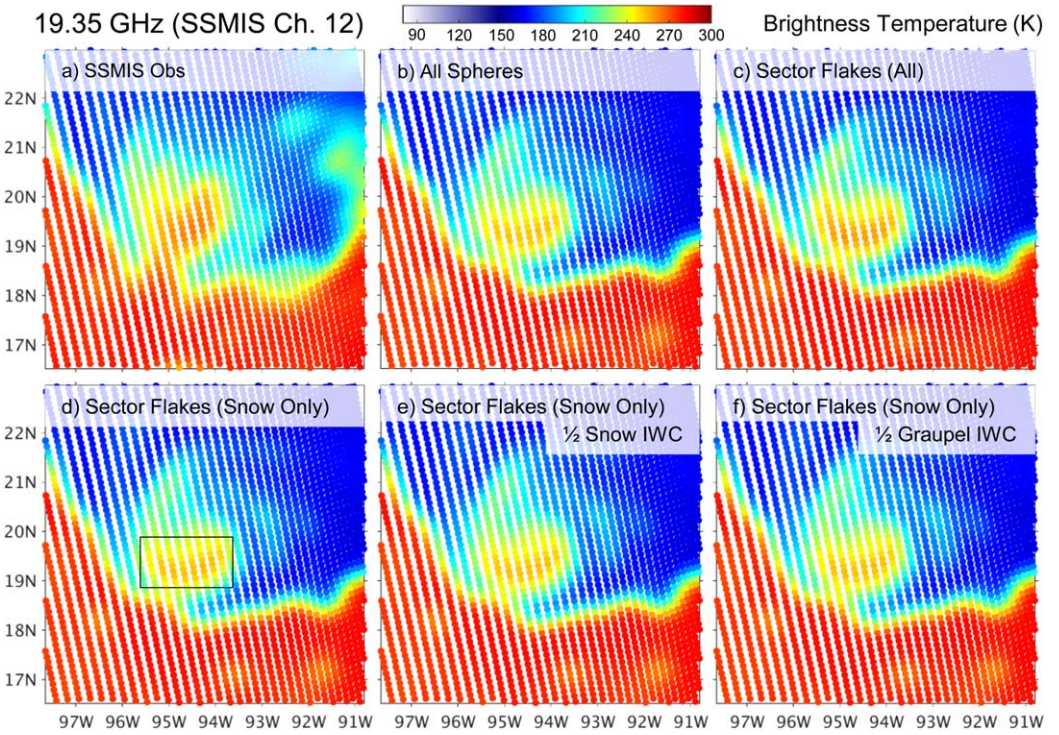

Figure 5. Same as Figure 3 but for SSMIS channel 12 (19.35 GHz). The box in (d) indicates the broad area of moderate to high liquid water path collocated with some graupel.

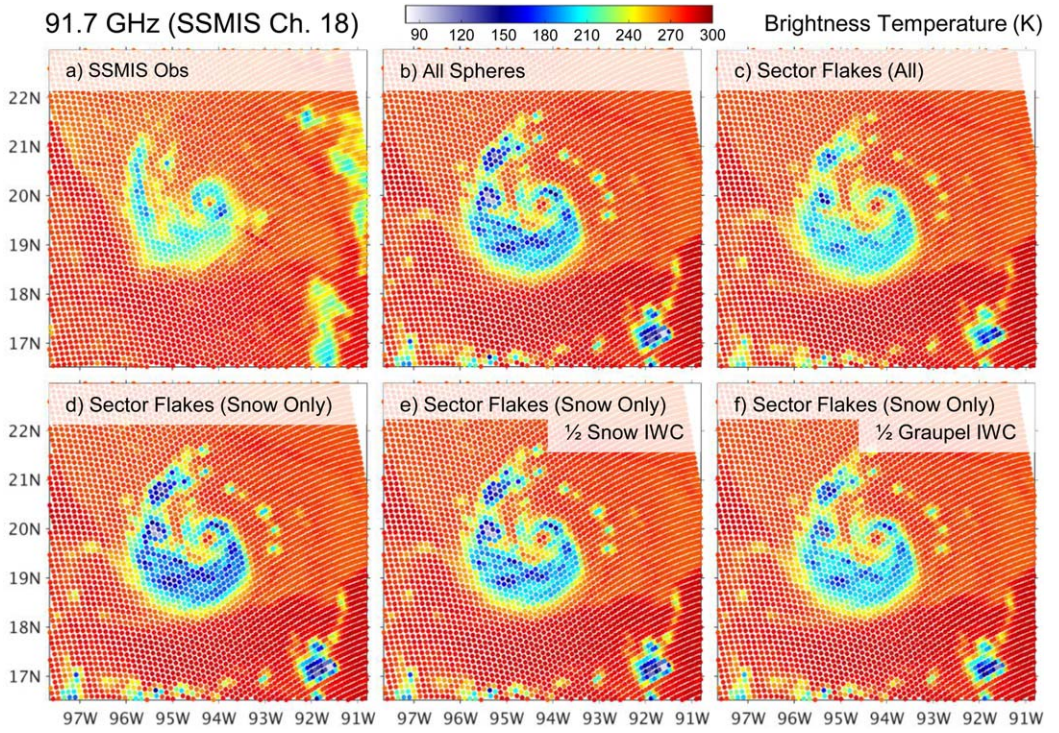

Figure 6. Same as Figure 3 but for SSMIS channel 18 (91.7 GHz).

Table 1
Summary Description of All CRTM Experiments and Domain-Average Brightness Temperatures of the Simulations and SSMIS Observations

Figures 3–6	Snow	Graupel	Halved Ice Water Content	Domain-average brightness temperature (K) 0100 UTC 17 September			
				Ch. 12 (19.35H)	Ch. 15 (37H)	Ch. 18 (91.7H)	Ch. 9 (183 ± 7)
a	SSMIS observations			223.1	233.1	267.8	254.9
b	Spheres	Spheres	None	213.7	222.5	267.3	257.5
c	Sectors	Sectors	None	214.3	224.6	268.7	250.9
d	Sectors	Spheres	None	213.8	222.8	266.1	250.7
e	Sectors	Spheres	Snow	213.8	222.9	267.7	254.2
f	Sectors	Spheres	Graupel	214.2	223.8	267.9	251.3
N.A.	Dendrites	Spheres	None	213.8	222.9	268.1	256.1
N.A.	Long columns	Spheres	None	213.7	221.6	256.7	243.0
N.A.	Thin plates	Spheres	None	213.7	221.6	260.1	246.6
N.A.	3-bullet rosettes	Spheres	None	213.8	222.7	265.3	250.5
N.A.	6-bullet rosettes	Spheres	None	213.8	222.7	266.2	252.5
N.A.	Sphere-equivalents of sectors	Spheres	None	213.8	222.9	268.6	257.8

substituting spheres with sector snowflakes would cause less upwelling radiation from the surface and lower troposphere to exit the top of the atmosphere, thus brightness temperatures would be lower. The higher absorption coefficients for sector snowflakes shown in Figure 2 are also consistent with the simulation results, but the absorption coefficients are more than an order of magnitude smaller than the scattering coefficients at

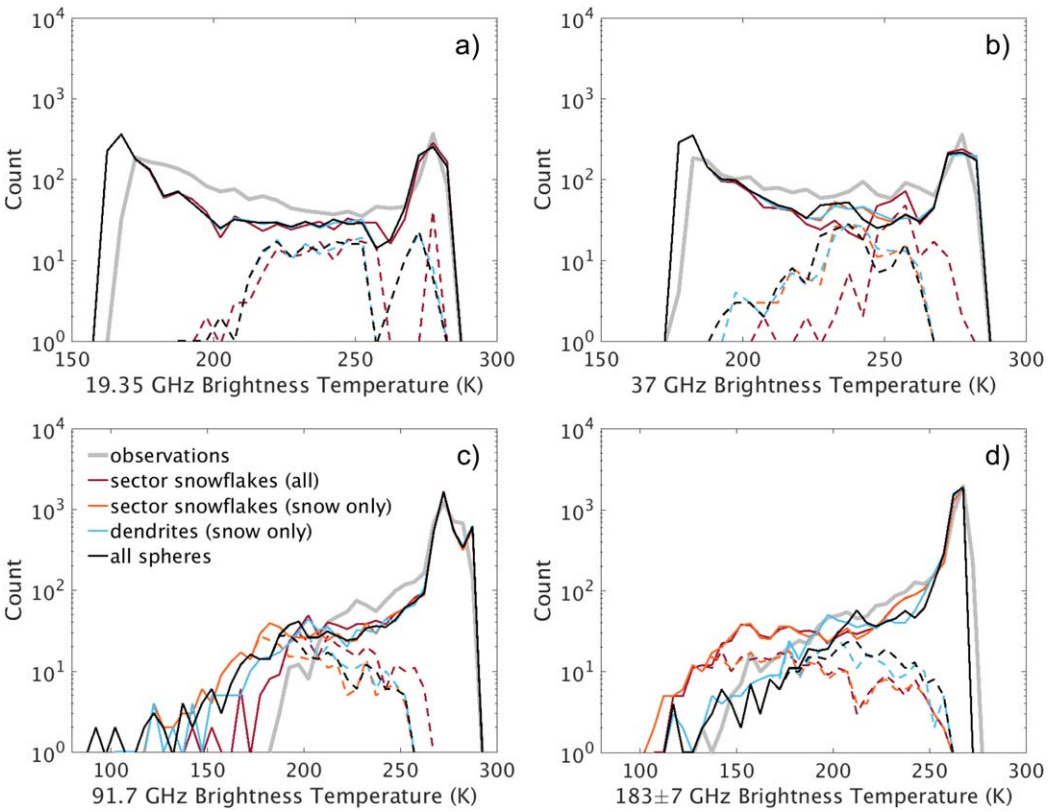

Figure 7. Histograms of observed and CRTM (17 September 0100 UTC) brightness temperatures from four experiments with different cloud scattering properties. Solid lines include all locations, while dashed lines include only locations with an average graupel water path greater than 1 kg m^{-2}. All bin widths are 5 K. Note that for 19.35 GHz "sector snowflakes (snow only)" has nearly identical results to "dendrites (snow only)."

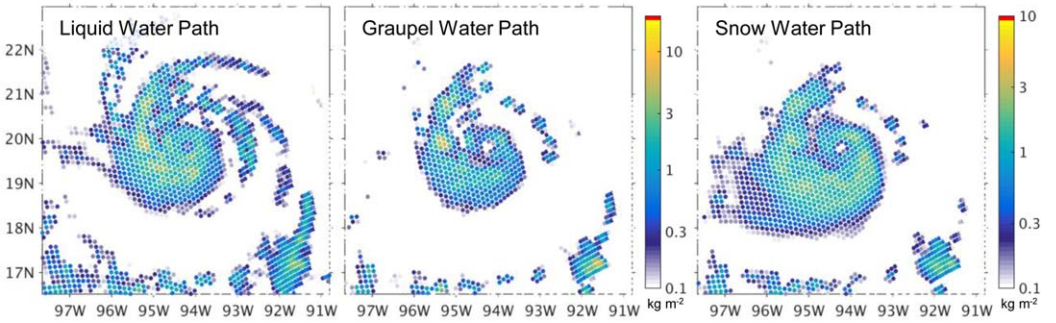

Figure 8. Water paths (kg m^{-2}) of (a) liquid (sum of rain and cloud liquid water), (b) graupel, and (c) snow from the WRF simulation at 0100 UTC 17 September. The same Gaussian-weighted averaging for SSMIS 91.7 GHz simulated brightness temperatures is applied to the native 3 km grid spacing of the model fields.

most water contents. Using sector snowflake particle scattering properties for snow results in a substantial cold bias to observations (Figure 3d versus Figure 3a), but reducing the snow water contents by half raises these cold-biased brightness temperatures by a domain-average of 3.5 K (Figure 3e versus Figure 3d). Much of this difference is from the areas of light to moderate snow water content of the southwest outflow of the hurricane, which is hardly evident in the spherical particle simulation. By comparison, reducing graupel water contents by half raises the average brightness temperature by just 0.6 K (Figure 3f versus Figure 3d). Furthermore, replacing graupel spheres of bulk density 500 kg m^{-3} with sector snowflakes (Figure 3c versus Figure 3d) raises domain-averaged brightness temperatures by only 0.28 K. This replacement causes small changes in brightness temperature bin counts throughout the range 100–265 K (Figure 7d); at the higher brightness temperatures, there are nearly 800 locations seeing miniscule (less than 0.02 K) decreases.

For channel 15 (37 GHz; Figures 4 and 7b), the overall results are nearly the complete opposite from 183 GHz. CRTM-DS gives a cold bias to observed brightness temperatures in the hurricane precipitation area (Figure 4b versus Figure 4a, much less area of orange), and graupel is primarily responsible for this bias. At 37 and 19.35 GHz, among other low frequencies, the primary signal from all hydrometeors above water surfaces (which have low emissivity and therefore low brightness temperature in clear sky, unlike land surfaces) is the increase in brightness temperatures from net addition of radiation by the liquid water content. But in these 37 GHz simulations with spherical graupel particles, the scattering by graupel leads to widespread and substantial decreases in brightness temperatures. In the area of the highest graupel water contents (box in Figure 4b), the brightness temperature is comparable to that in areas of generally clear sky over water (e.g., northern half of the eastern-most extent of the simulation domain). There is a significant increase in precipitation-affected simulated brightness temperatures when replacing graupel spheres with sector snowflakes (Figure 4c versus Figure 4d), amounting to a domain-average increase of 1.8 K. The decrease of occurrences of brightness temperatures between 190 and 245 K and the increase of occurrences between 245 and 285 K has a significant contribution from locations with more than 1 kg m^{-2} of graupel (Figure 7b). The top row of Figure 2 shows that using sector snowflake scattering properties for the graupel species leads to scattering coefficients of about an order of magnitude less than using spheres, which is consistent with this increase in brightness temperatures. When using spherical particle scattering properties for graupel, halving the input graupel water contents is also effective at raising brightness temperatures (Figure 4f versus Figure 4d). In contrast to graupel, the presence and representation of snow has little impact on brightness temperatures at 37 GHz. Substituting spheres with sector snowflakes for only the snow species slightly warms the brightness temperatures in some areas of precipitation (Figure 4d versus Figure 4b), but many areas of relatively low brightness temperatures (compared to neighboring spatial regions) with high graupel water content are relatively unchanged (Figure 7b). Reducing the snow water contents by half also has little warming effect (Figure 4e versus Figure 4d).

The relative impacts of snow and graupel in simulated brightness temperatures for channel 12 (19.35 GHz; Figures 5 and 7a) are similar to that with channel 15. Fortunately, there are no locations of heavy precipitation with high graupel water contents having simulated brightness temperatures as low as clear-sky (or low liquid water content) areas over the ocean. However, a similar ambiguity between lower liquid water content and higher graupel water content exists. Switching from spherical graupel to sector snowflake graupel raises the brightness temperatures in many locations across the hurricane precipitation area (box in Figure

5d versus same area in Figures 5c and 7a) by nearly as much as completely excluding both snow and graupel from the CRTM (not shown).

The water contents and particle types of both snow and graupel have meaningful impacts on brightness temperatures for channel 18 (91.7 GHz; Figures 6 and 7c), but changes to graupel have the greater impact. Halving graupel water contents raises domain-average brightness temperatures by 1.8 K, compared to a 1.6 K increase from halving snow water contents (Figure 6f versus Figure 6e). Compared to using spheres for both snow and graupel, using sector snowflakes for only snow decreases domain-average brightness temperatures by just 1.2 K, while using sector snowflakes for both snow and graupel increases brightness temperatures by 2.6 K (compare Figures 6c–6e). The differences in cloud scattering properties, and their effects on brightness temperatures, between the different treatments of graupel are consistent with what was noted at 37 GHz. The experimental changes to snow produce brightness temperature results similar to what was seen at 183 GHz. However, unlike at 183 GHz, spheres and sector snowflakes produce similar values of snow scattering coefficients at 91.7 GHz (not shown). Therefore, differences in 91.7 GHz brightness temperatures are likely caused primarily by the differences in the directionality of the scattering.

Only the use of spheres for both snow and graupel leads to simulated brightness temperatures at 91.7 GHz which are colder than that at 183 GHz in the area of the hurricane precipitation (Figure 3b versus Figure 6b). Also, all of the CRTM simulations at 91.7 GHz (Figure 6) have a cold bias to observations, even as the use of randomly oriented cloud and precipitation particles should be a source of positive bias to observations in 91.7 GHz simulations at horizontal polarization (e.g., Defer et al., 2014; Gong & Wu, 2017).

Figure 9 shows that the afore-mentioned similarities and differences in brightness temperatures between the different experiments are consistent throughout much of the simulation period. As evidenced here and in the brightness temperature plots, the use of sector snowflakes for snow results in brightness temperatures (in areas of precipitation) which are lower than observations at all four frequencies.

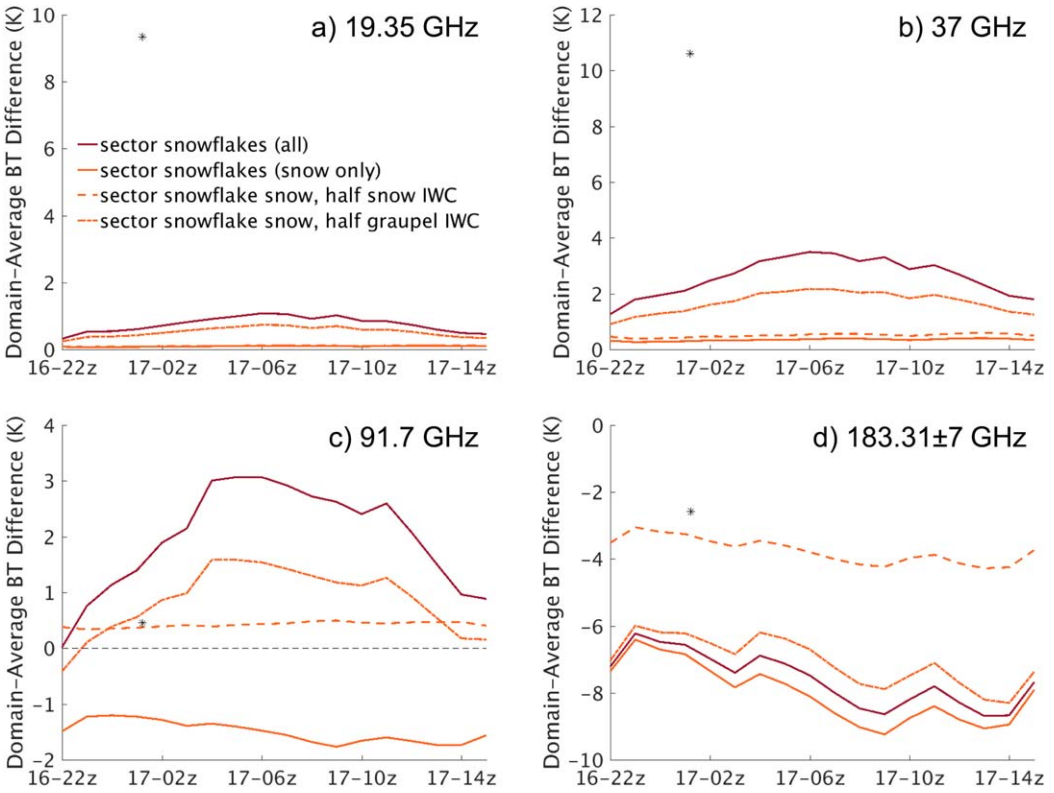

Figure 9. Time series of domain-average differences in CRTM brightness temperature obtained by subtracting the average obtained by using spheres to represent all cloud scattering properties from the averages obtained from the sector snowflake experiments. The differences of the domain-average of the F16 SSMIS observed brightness temperatures at 0117 UTC from the sphere-only results are indicated by the stars in the four plots.

The greatest differences between simulated and observed brightness temperatures that remain occur at the lowest two frequencies. A significant contributor to the domain-average cold biases are the clear-sky scenes (already low in brightness temperature); at 19.35 GHz, all of the simulations have 589 locations with brightness temperatures under 170 K, while the observations have only 32 such locations (see Figure 7a). But even considering only the areas of hurricane precipitation over the ocean, all of the experimental setups for precipitation ice produce cold-biased brightness temperatures (which is also true if completely removing all snow and graupel; not shown). The absence of melting particles in the radiative transfer could be responsible for cold biases of this magnitude (e.g., Bauer, 2001). The bias can also be removed by not using spherical graupel particles and increasing the liquid water content (results not shown).

4.2. Other Representations for the Snow Species

As previously discussed, replacement of the spherical particles specified by the microphysics scheme (CRTM-DS) with nonspherical particles also changes the particle size distribution and the mass of individual particles of a given maximum dimension. The influence on brightness temperatures of the different particle shapes can be tested in isolation from these other changes by replacing every nonspherical particle with its spherical-equivalent (equal maximum dimension and mass). Compared with the CRTM-DS spheres (all with bulk density 100 kg m^{-3}), the small sphere-equivalent particles of the bullet rosettes and snowflakes will be denser and less numerous, and the large particles will be less dense and more numerous.

Similar to Figure 9, Figure 10 shows time series of domain-average brightness temperature differences relative to spheres as specified by the microphysics scheme (CRTM-DS; all spheres with bulk density 100 kg m^{-3}) at each of the four frequencies of interest, but for a wide variety of particle representations of only the snow species. These representations are the long columns, thin plates, 3-bullet rosettes, 6-bullet rosettes, dendrites, sector snowflakes, and the spherical-equivalents of sector snowflakes. Figure 11 shows 0100 UTC 17 September brightness temperatures at 37, 91.7, and 183 GHz resulting from the use of three

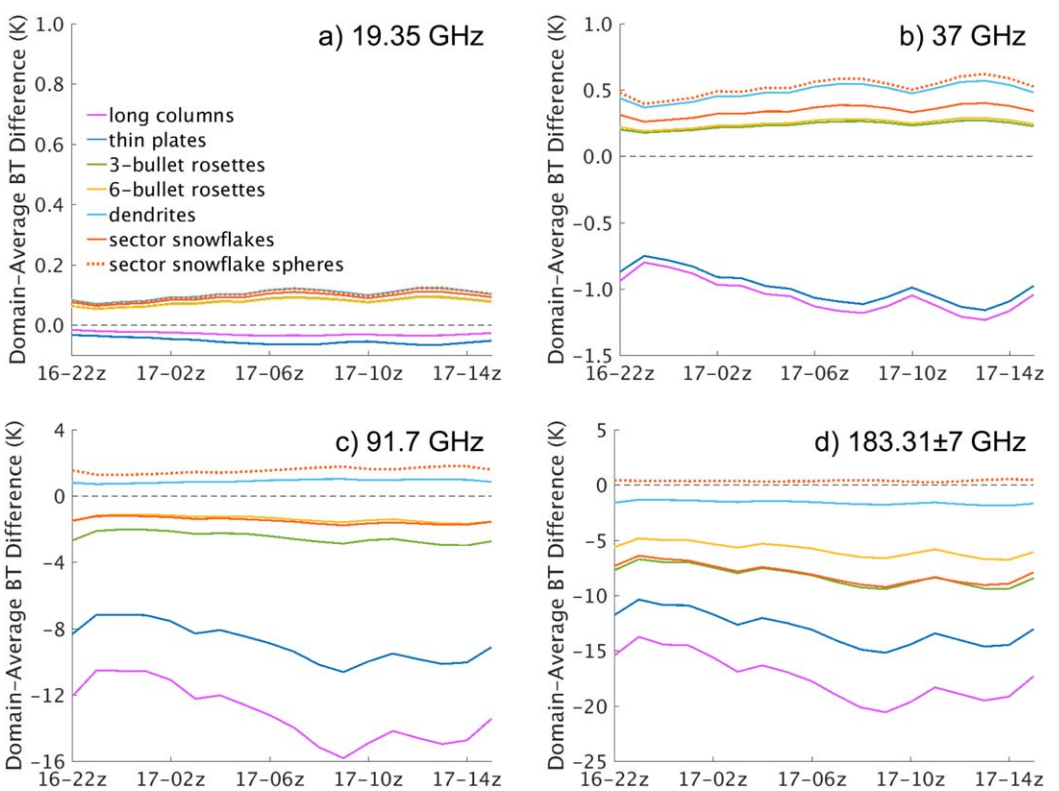

Figure 10. Similar to Figure 9, but with domain-average CRTM brightness temperature differences between results obtained using different nonspherical particle types for the snow species and the spheres specified by the WSM6 microphysics scheme.

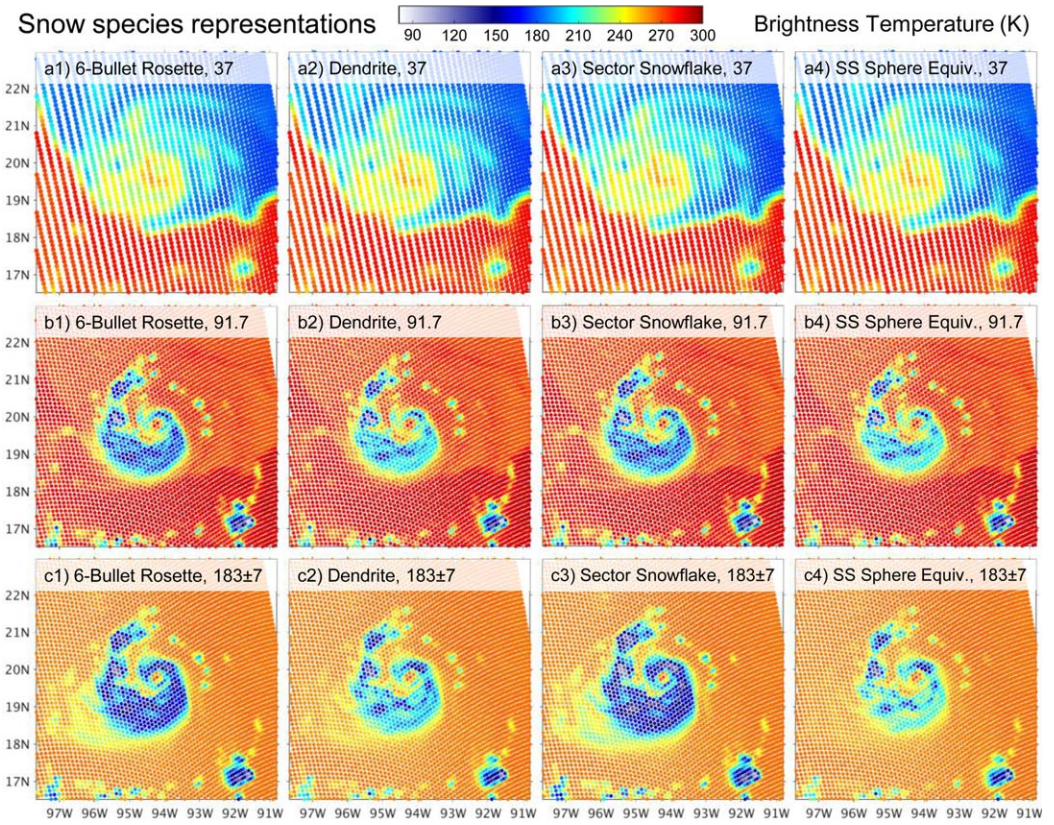

Figure 11. CRTM-simulated brightness temperatures (K) at (a) 37 GHz, (b) 91.7 GHz, and (c) 183 ± 7 GHz with snow represented as (1) 6-bullet rosettes, (2) dendrites, (3) sector snowflakes, and (4) the spherical-equivalent particles of the sector snowflakes.

of the nonspherical particle types and spherical-equivalents of sector snowflakes. As seen in Figures 9a and 10a, there is virtually no impact on 19.35 GHz brightness temperatures based on the treatment of snow, hence the omission of this channel in Figure 11.

The spherical-equivalents of sector snowflakes produce results more similar to the spherical particles in CRTM-DS than the actual sector snowflakes. While the sector snowflakes themselves produce significantly lower brightness temperatures than CRTM-DS at the frequencies with substantial sensitivity to the treatment of snow (91.7 and 183 GHz; Figures 10c and 10d), sector snowflake spherical-equivalent particles produce slightly higher brightness temperatures than CRTM-DS. However, the sector snowflake spherical-equivalent particles improve upon the warm bias of 91.7 GHz relative to 183 GHz compared to CRTM-DS by a domain-average of 1.0 K.

Unlike either collection of spheres, all six of the nonspherical particle types shown (as well as the three other columns and plates, and two other rosettes) produced lower average brightness temperatures at 183 GHz than at 91.7 GHz in the precipitation area of the hurricane. The columns and plates led to the overall worst results, producing by a wide margin the lowest brightness temperatures and largest differences to observations. Using dendrites, 183 GHz brightness temperatures were still too high relative to 91.7 GHz brightness temperatures in precipitation-affected areas compared to observations (compare the simulation differences illustrated in Figures 11c2 and 11b2 to the observation differences illustrated in Figures 3a and 6a). Besides columns and plates, the 3-bullet rosettes produced the lowest brightness temperatures at 91.7 GHz. The slight differences in domain-average brightness temperatures at 37 GHz seen in Figures 10 and 11 primarily exist in the bands containing appreciable liquid water content but no appreciable graupel water content (see Figures 8a and 8b).

Between the use of dendrites and the bullet rosettes, there is consistency across the 183 and 91.7 GHz brightness temperatures with respect to the relative impacts on brightness temperatures: the relative

distance between each of the lines in Figure 10 is nearly the same in both plots, with the brightness temperatures from using 6-bullet rosettes being below that of dendrites and above, and slightly closer to, 3-bullet rosettes. However, with sector snowflakes, average brightness temperatures are barely below 6-bullet rosettes at 91.7 GHz, and barely above 3-bullet rosettes at 183 GHz. Sector snowflakes appear to have distinct impacts on the radiative transfer across the higher frequencies.

5. Concluding Remarks

In our previous work (Sieron et al., 2017), cloud scattering lookup tables for the CRTM were constructed to be consistent with the particle properties (i.e., homogeneous spheres) and size distributions specified by the WSM6 microphysics scheme. New cloud scattering lookup tables for snow and graupel species are constructed here, replacing spherical particles with nonspherical particles of equal size, but adjusting the particle size distribution to maintain the WSM6 specification of total mass with respect to particle size, $M(D)$.

In this case study, simulated brightness temperatures of Hurricane Karl (2010) support the use of sector snowflakes to represent the snow species in substitution of the 100 kg m^{-3} ice spheres specified by WSM6. The use of sector snowflakes is most effective at reducing the brightness temperatures at 183 GHz relative to the brightness temperatures at 91.7 GHz in precipitation-affected areas. The 3-bullet rosette is the next most effective particle type, while dendrites are the least effective of the tested nonspherical particles. Additionally, sector snowflakes produce higher brightness temperatures than 3-bullet rosettes (but lower brightness temperatures than dendrites) at all of the tested frequencies.

Sector snowflake scattering properties produced cold biases relative to observations in simulations at both 91.7 and 183 GHz, suggesting a positive bias in model snow water contents. In contrast, using spheres to represent snow produced a cold bias at 91.7 GHz (suggesting too much snow), but a warm bias at 183 GHz (suggesting too little snow). Perhaps the randomly oriented sector snowflake is the best of the Liu (2008) particle types at approximating the microwave scattering and absorption properties of the aggregates of columns and other ice particles observed most in tropical cyclones (Houze, 2010), while spheres of bulk density 100 kg m^{-3} are likely among the least appropriate.

The use of sector snowflakes for graupel is effective at removing the cold bias at the lower frequencies, such as 37 and 19.35 GHz. However, the sector snowflake is not nearly as physically realistic a representation of real graupel particles as compared to homogeneous soft spheres. Graupel particles grow primarily by accretion of smaller cloud droplets, and a homogeneous mixture of ice and air may not be an unreasonable model of such a particle. A sphere may also be a decent representation of the shape of some graupel particles; however, no graupel particle is a perfect and homogeneous sphere, and the symmetry of a sphere produces unique scattering properties. It may be worthwhile investigating other particle constructions similar to the form of graupel, such as conically shaped homogeneous ice-air mixtures or more detailed constructions of accretion growth onto a snow particle, which may provide more accurate scattering property representations for graupel. Without such particle constructions to test in the database selected for this study, the soft sphere is recommended for representing graupel. The resulting cold biases of simulated brightness temperatures at low frequencies can be resolved by reducing graupel water contents by half or more.

The utilization of the Liu (2008) sector snowflake to represent the microwave scattering and absorption properties of snow, or even all ice precipitation, continues to gain support in the community. Geer and Baordo (2014) also found that the sector snowflake is the best particle type for removing RTTOV-SCATT radiative transfer model simulation biases to observations when applied to ECMWF 4D-Var data assimilation output (which has only a snow precipitation ice species). Galligani et al. (2017) found that the sector snowflake (or dendrite) particle type applied to both snow and graupel in WSM6 simulations produced the least scattering and closest brightness temperatures to observations at high frequencies. Eriksson et al. (2015) further demonstrate that the sector snowflake is the nonspherical particle construction with appropriately moderate scattering and absorption properties relative to other particle shapes, and support its use as a proxy for representing precipitation ice in microwave radiative transfer simulations in (all-too frequent) conditions with insufficient constraint on particle shapes.

In addition to considering the representativeness of certain particle shapes, these analyses of snow and graupel scattering properties are based on the pragmatic perspective of presuming that regional-scale

models produce too much ice (e.g., Garvert et al., 2005; Han et al., 2013; Milbrandt et al., 2008; Morrison et al., 2015). If the primary metric was not the differences between 91.7 and 183 GHz brightness temperatures, but instead simply the average closeness to fit to observations across all tested frequencies with the given water contents (as in Geer & Baordo, 2014), then these results would offer the most support toward using dendrites for the snow species. But with little to no direct observations of ice particle shapes and water contents throughout a volume in a microwave radiance measurement, it is challenging, if not impossible, to independently verify that both the modeled water contents and the assumptions made in calculating cloud scattering properties correspond well to reality.

This study employed a particle replacement method which preserves the total mass of a particle population with respect to size, in part because this preserves the formulaic relationship between water content and fall speed in the model microphysics. In reality, homogeneous spherical particles would generally fall at different speeds than nonspherical particles of the same maximum dimension. However, in most microphysics schemes, including WSM6, the fall speed parameter values are empirically derived from observed real particle shapes and size distributions (e.g., Locatelli & Hobbs, 1974; Matson & Huggins, 1980). Therefore, the microphysics modeled fall speeds are already mismatched from the microphysics particle properties and size distributions. This preexisting inconsistency within the microphysics scheme could be interpreted as removing strict obligations to adjust the model fall speed parameters when changing the shapes of particles in the modeled radiative transfer. The significance of consistent particle representations—whether with spherical or nonspherical particles—between radiative transfer models and fall speed calculations may depend on application but is certainly worthy of future investigation.

As discussed in section 2, nonspherical particles for the ice cloud species were not tested, in part because of minimal impacts of soft sphere cloud ice on simulated brightness temperatures. This is due to a combination of low water paths and of the simulated wavelengths being large relative to the monodisperse particle diameters, which are prescribed to be less than 0.5 mm. The WSM6 scheme has three primary equations relating water content to the number concentration, particle size (monodisperse) and particle mass (see Sieron et al., 2017, their Appendix A2). These parametric relationships, along with imposed minima and maxima in parameter values, create four "regimes" of water content values, between which there are significant changes in the relationship between water content and particle size/mass. For example, in the regime of ice cloud water contents greater than 0.0172 kg m^{-3}, both the number concentration and diameter of ice cloud particles are fixed (10^6 m^{-3} and 0.5 mm, respectively), with only the particle mass changing with water content. Using spheres of the bulk density appropriate for the specified particle size and mass will logically represent these ice clouds, but using just one nonspherical particle shape of this size cannot. If these concerns with WSM6 were addressed or set aside, or if considering a different microphysics scheme, then the use of nonspherical particles for ice clouds is an interesting prospect for improved correspondence of simulations to observations, as nonspherical ice cloud particles could further disproportionally reduce brightness temperatures at 183 GHz relative to 91.7 GHz.

The latest generation of microphysics schemes predict graupel bulk density (e.g., Milbrandt & Morrison, 2013) or similar information (e.g., Morrison & Milbrandt, 2015), or ice particle habits (e.g., Sulia et al., 2014). This is information that could be used to more seamlessly map nonspherical particle scattering property calculations to outputs of these microphysics schemes.

The WSM6 microphysics-consistent cloud scattering properties using sector snowflakes for the snow species is being used in the Community Radiative Transfer Model (CRTM) as the forward operator for PSU-WRF Ensemble Kalman Filter (EnKF) data assimilation experiments for tropical cyclones (e.g., Zhang et al., 2016; Zhang & Weng, 2015). In addition to working toward improving analyses and forecasts, these experiments will also serve to test hypotheses relating to excess snow and graupel water contents in current WSM6 outputs.

Acknowledgments
This research is partially supported by NASA grants NNX16AD84G and NNX12AJ79G, and ONR grant N000140910526. S.B.S. was also supported by the National Science Foundation Graduate Research Fellowship under grant DGE1255832. The authors thank Guosheng Liu for providing the nonspherical particle scattering property database via open public access and documenting it in detail via Liu (2008). Coauthor and high school student Lily N. Zhang participated in a 3 month summer research internship conducting preliminary analyses of the Liu database and producing samples of microphysics-consistent cloud scattering coefficients and phase functions. Discussions with Guosheng Liu, Fuzhong Weng, Qinghua Liu, Ben Johnson, Xiaolei Zou, Alan Geer, and many others were beneficial to this study. Computing was provided by the Texas Advanced Computing Center (TACC). The SSMIS observations are sourced from the Colorado State University (CSU) Fundamental Climate Data Record (FCDR). The WRF model output can be accessed at http://hfip.psu.edu/sbs5130/SieronEtAl2018_JAMES_data.tar.gz.

References

Alvey, G. R., Zawislak, J., & Zipser, E. (2015). Precipitation properties observed during tropical cyclone intensity change. *Monthly Weather Review*, *143*, 4476–4492.

Baran, A., Bodas-Salcedo, A., Cotton, R., & Lee, C. (2011). Simulating the equivalent radar reflectivity of cirrus at 94 GHz using an ensemble model of cirrus ice crystals: A test of the Met Office global numerical weather prediction model. *Quarterly Journal of the Royal Meteorological Society*, *137*, 1547–1560. https://doi.org/10.1002/qj.870

Bauer, P. (2001). Over-ocean rainfall retrieval from multisensor data of the tropical rainfall measuring mission. Part I: Design and evaluation of inversion databases. *Journal of Atmospheric and Oceanic Technology*, *18*, 1315–1330.
Bennartz, R. (2000). Optimal convolution of AMSU-B to AMSU-A. *Journal of Atmospheric and Oceanic Technology*, *17*, 1215–1225.
Brueske, K. F., & Velden, C. S. (2003). Satellite-based tropical cyclone intensity estimation using the NOAA-KLM series Advanced Microwave Sounding Unit (AMSU). *Monthly Weather Review*, *131*, 687–697. https://doi.org/10.1175/1520-0493(2003)131<0687:SBTCIE>2.0.CO;2
Defer, E., Galligani, V. S., Prigent, C., & Jimenez, C. (2014). First observations of polarized scattering over ice clouds at closeto-millimeter wavelengths (157 GHz) with MADRAS on board the Megha-Tropiques mission. *Journal of Geophysical Research: Atmospheres*, *119*, 12301–12316. https://doi.org/10.1002/2014JD022353
Dudhia, J., Hong, S. Y., & Lim, K. S. (2008). A new method for representing mixed-phase particle fall speeds in bulk microphysics parameterizations. *Journal of the Meteorological Society of Japan*, *86A*, 33–44. https://doi.org/10.2151/jmsj.86A.33
Eriksson, P., Jamali, M., Mendrok, J., & Buehler, S. A. (2015). On the microwave optical properties of randomly oriented ice. *Atmospheric Measurement Techniques*, *8*, 1913–1933.
Galligani, V. S., Wang, D., Imax, M. A., Salio, P., & Prigent, C. (2017). Analysis and evaluation of WRF microphysics schemes for deep moist convection over south-eastern South America (SESA) using microwave satellite observation and radiative transfer simulations. *Atmospheric Measurement Techniques*, *10*, 3627–3649. https://doi.org/10.5194/amt-10-3627-2017
Garvert, M. F., Woods, C. P., Colle, B. A., Mass, C. F., Hobbs, P. V., Stoelinga, M. T., et al. (2005). The 13–14 December 2001 IMPROVE-2 event. Part II: Comparisons of MM5 model simulations of clouds and precipitation with observations. *Journal of the Atmospheric Sciences*, *62*, 3520–3534.
Geer, A. J., & Baordo, F. (2014). Improved scattering radiative transfer for frozen hydrometeors at microwave frequencies. *Atmospheric Measurement Techniques*, *7*, 1839–1860. https://doi.org/10.5194/amt-7-1839-2014
Gong, J., & Wu, D. L. (2017). Microphysical properties of frozen particles inferred from Global Precipitation Measurement (GPM) Microwave Imager (GMI) polarimetric measurements. *Atmospheric Chemistry and Physics*, *17*, 2741–2757. https://doi.org/10.5194/acp-17-2741-2017
Greenwald, T., Bennartz, R., O'Dell, C., & Heidinger, A. (2004). Fast computation of microwave radiances for data assimilation using the successive order of scattering approximation. *Journal of Applied Meteorology*, *44*, 960–966. https://doi.org/10.1175/JAM2239.1
Haddad, Z. S., Steward, J. L., Tseng, H.-C., Vukicevic, T., Chen, S.-H., & Hristova-Veleva, S. (2015). A data assimilation technique to account for the nonlinear dependence of scattering microwave observations of precipitation. *Journal of Geophysical Research: Atmospheres*, *120*, 5548–5563. https://doi.org/10.1002/2015JD023107
Han, M., Braun, S. A., Matsui, T., & Williams, C. R. (2013). Evaluation of cloud microphysics schemes in simulations of a winter storm using radar and radiometer measurements. *Journal of Geophysical Research: Atmospheres*, *118*, 1401–1419. https://doi.org/10.1002/jgrd.50115
Han, Y., van Delst, P., Liu, Q., Weng, F., Yan, B., Treadon, R., et al. (2006). *JCSDA Community Radiative Transfer Model (CRTM)—Version 1* (NOAA Tech. Rep., Vol. *122*). Silver Spring, MD: National Oceanic and Atmospheric Administration.
Harnos, D. S., & Nesbitt, S. W. (2016). Passive microwave quantification of tropical cyclone inner-core cloud populations relative to subsequent intensity change. *Monthly Weather Review*, *144*, 4461–4482. https://doi.org/10.1175/MWR-D-15-0090.1
Hogan, R. J., Tian, L., Brown, P. R., Westbrook, C. D., Heymsfield, A. J., & Eastment, J. D. (2012). Radar scattering from ice aggregates using the horizontally aligned oblate spheroid approximation. *Journal of Applied Meteorology and Climatology*, *51*, 655–671. https://doi.org/10.1175/JAMC-D-11-074.1
Hong, G. (2007). Parameterization of scattering and absorption properties of nonspherical ice crystals at microwave frequencies. *Journal of Geophysical Research*, *112*, D11208. https://doi.org/10.1029/2006JD008364
Houze, R. A. (2010). Clouds of tropical cyclones. *Monthly Weather Review*, *138*, 293–344.
Kazumori, M., Geer, A. J., & English, S. J. (2016). Effects of all-sky assimilation of GCOM-W/AMSR2 radiances in the ECMWF numerical weather prediction system. *Quarterly Journal of the Royal Meteorological Society*, *142*, 721–737.
Kulie, M. S., Bennartz, R., Greenwald, T. J., Chen, Y., & Weng, F. (2010). Uncertainties in microwave properties of frozen precipitation: Implications for remote sensing and data assimilation. *Journal of the Atmospheric Sciences*, *67*, 3471–3487.
Lang, S., Tao, W.-K., Cifelli, R., Olson, W., Halverson, J., Rutledge, S., et al. (2007). Improving simulations of convective system from TRMM LBA: Easterly and Westerly regimes. *Journal of the Atmospheric Sciences*, *64*, 1141–1164. https://doi.org/10.1175/JAS3879.1
Li, X., Tao, W.-K., Matsui, T., Liu, C., & Masunaga, H. (2010). Improving a spectral bin microphysical scheme using long-term TRMM satellite observations. *Quarterly Journal of the Royal Meteorological Society*, *136*, 382–399.
Liu, G. (2004). Approximation of single scattering properties of ice and snow particles for high microwave frequencies. *Journal of the Atmospheric Sciences*, *61*, 2441–2456.
Liu, G. (2008). A database of microwave single-scattering properties for nonspherical ice particles. *Bulletin of the American Meteorological Society*, *89*(10), 1563–1570. https://doi.org/10.1175/2008BA MS2486.1
Liu, Q., & Weng, F. (2006). Combined Henyey-Greenstein and Rayleigh phase function. *Applied Optics*, *45*, 7475–7479.
Locatelli, J., & Hobbs, P. (1974). Fall speeds and masses of solid precipitation particles. *Journal of Geophysical Research*, *79*, 2185–2197.
Madhulatha, A., George, J. P., & Rajagopal, E. N. (2017). All-sky radiance simulation of Megha-Tropiques SAPHIR microwave sensor using multiple scattering radiative transfer model for data assimilation applications. *Journal of Earth System Science*, *126*, 24. https://doi.org/10.1007/s12040-017-0805-3
Masunaga, H., Matsui, T., Tao, W.-k., Hou, A. Y., Kummerow, C. D., Nakajima, T., et al. (2010). Satellite data simulator unit: A multisensor, multispectral satellite simulator package. *Bulletin of the American Meteorological Society*, *91*, 1625–1632. https://doi.org/10.1175/2010BAMS2809.1
Matson, R. J., & Huggins, A. W. (1980). The direct measurement of the sizes, shapes, and kinematics of falling hailstones. *Journal of the Atmospheric Sciences*, *37*, 1107–1125. https://doi.org/10.1175/1520-0469(1980)037 < 1107:TDMOTS>2.0.CO;2
Matsui, T., Chern, J., Tao, W.-K., Lang, S., Satoh, M., Hashino, T., et al. (2016). On the land-ocean contrast of tropical convection and microphysics statistics derived from TRMM satellite signals and global storm-resolving models. *Journal of Hydrometeorology*, *17*, 1425–1445. https://doi.org/10.1175/JHM-D-15-0111.1
Melhauser, C., Zhang, F., Weng, Y., Jin, Y., Jin, H., & Zhao, Q. (2017). A multiple-model convection-permitting ensemble examination of the probabilistic prediction of tropical cyclones: Hurricanes Sandy (2012) and Edouard (2014). *Weather and Forecasting*, *32*, 665–688.
Meissner, T., & Wentz, F. J. (2009). Wind-vector retrievals under rain with passive satellite microwave radiometers. *IEEE Transactions on Geoscience and Remote Sensing*, *47*, 3065–3083. https://doi.org/10.1109/TGRS.2009.2027012
Milbrandt, J. A., & Morrison, H. (2013). Prediction of graupel density in a bulk microphysics scheme. *Journal of the Atmospheric Sciences*, *70*, 410–429. https://doi.org/10.1175/JAS-D-12-0204.1
Milbrandt, J. A., Yau, M. K., Mailhot, J., & Bélair, S. (2008). Simulation of an orographic precipitation event during IMPROVE-2. Part I: Evaluation of the control run using a triple-moment bulk microphysics scheme. *Monthly Weather Review*, *136*, 3873–3893. https://doi.org/10.1175/2008MWR2197.1

Mitchell, D. L. (1991). Evolution of snow-size spectra in cyclonic storms. Part II: Deviations from the exponential form. *Journal of the Atmospheric Sciences*, *48*, 1885–1899.

Morrison, H., Milbrandt, J. A. (2015). Parameterization of cloud microphysics based on the prediction of bulk ice particle properties. Part I: Scheme description and idealized tests. *Journal of the Atmospheric Sciences*, *72*, 287–311. https://doi.org/10.1175/JAS-D-14-0065.1

Morrison, H., Milbrandt, J. A., Bryan, G. H., Ikeda, K., Tessendorf, S. A., & Thompson, G. (2015). Parameterization of cloud microphysics based on the prediction of bulk ice particle properties. Part II: Case study comparisons with observations and other schemes. *Journal of the Atmospheric Sciences*, *72*, 312–339. https://doi.org/10.1175/JAS-D-14-0066.1

Morrison, H., Thompson, G., & Tatarskii, V. (2009). Impact of cloud microphysics on the development of trailing stratiform precipitation in a simulated squall line: Comparison of one- and two-moment schemes. *Monthly Weather Review*, *137*, 991–1007.

Nowell, H., Liu, G., & Honeyager, R. (2013). Modeling the microwave single-scattering properties of aggregate snowflakes. *Journal of Geophysical Research: Atmospheres*, *118*, 7873–7885. https://doi.org/10.1002/jgrd.50620

Reul, N., Chapron, B., Zabolotskikh, E., Donlon, C., Mouche, A., Tenerelli, J., et al. (2017). A new generation of tropical cyclone size measurements from space. *Bulletin of the American Meteorological Society*, *98*, 2367–2385. https://doi.org/10.1175/BAMS-D-15-00291.1

Rozoff, C. M., Velden, C. S., Kaplan, J., Kossin, J. P., & Wimmers, A. J. (2015). Improvements in the probabilistic prediction of tropical cyclone rapid intensification with passive microwave observations. *Weather and Forecasting*, *30*, 1016–1038. https://doi.org/10.1175/WAF-D-14-00109.1

Sieron, S. B., Clothiaux, E. E., Zhang, F., Lu, Y., & Otkin, J. A. (2017). Comparison of using distribution-specific versus effective radius methods for hydrometeor single-scattering properties for all-sky microwave satellite radiance simulations with different microphysics parameterization schemes. *Journal of Geophysical Research: Atmospheres*, *122*, 7027–7046. https://doi.org/10.1002/2017JD026494

Skamarock, W. C., Klemp, J., Dudhia, B. J., Gill, D. O., Barker, D. M., Duda, M. G., et al. (2008). *A description of the advanced research WRF version 3* (NCAR Tech. Note NCAR/TN-475+STR). Boulder, CO: National Center for Atmospheric Research.

Sulia, K. J., Morrison, H., & Harrington, J. Y. (2014). Dynamical and microphysical evolution during mixed-phase cloud glaciation simulated using the bulk adaptive habit prediction model. *Journal of the Atmospheric Sciences*, *71*, 4158–4180. https://doi.org/10.1175/JAS-D-14-0070.1

Surussavadee, C., & Staelin, D. H. (2007). Millimeter-wave precipitation retrievals and observed-versus-simulated radiance distributions: Sensitivity to assumptions. *Journal of the Atmospheric Sciences*, *64*, 3808–3826. https://doi.org/10.1175/2006JAS2045.1

Szyrmer, W., & Zawadzki, I. (2010). Snow studies. Part II: Average relationship between mass of snowflakes and their terminal fall velocity. *Journal of the Atmospheric Sciences*, *67*, 3319–3335. https://doi.org/10.1175/2010JAS3390.1

Weng, Y., & Zhang, F. (2012). Assimilating airborne Doppler radar observations with an ensemble Kalman filter for cloud-resolving hurricane initialization and prediction: Katrina (2005). *Monthly Weather Review*, *140*, 841–859. https://doi.org/10.1175/2011MWR3602.1

Yang, C., Liu, Z., Bresch, J., Rizvi, S. R. H., Yu Huang, X., & Min, J. (2016). AMSR2 all-sky radiance assimilation and its impact on the analysis and forecast of Hurricane Sandy with a limited-area data assimilation system. *Tellus, Series A*, *68*, 30917. https://doi.org/10.3402/tellusa.v68.30917

Zhang, F., Minamide, M., & Clothiaux, E. E. (2016). Potential impacts of assimilating all-sky infrared satellite radiances from GOES-R on convection-permitting analysis and prediction of tropical cyclones. *Geophysical Research Letters*, *43*, 2954–2963. https://doi.org/10.1002/2016GL068468

Zhang, F., & Weng, Y. (2015). Predicting hurricane intensity and associated hazards: A five-year real-time forecast experiment with assimilation of airborne Doppler radar observations. *Bulletin of the American Meteorological Society*, *96*, 25–32.